

# Supplementary materials to the paper *Topological defects of nematic liquid crystals confined in porous networks*

## 1 Laser micromachining

The microchannels were fabricated by femtosecond laser micromachining of fused silica glass substrates. The short duration of a femtosecond pulse leads to high peak powers and very high intensities even for low pulse energies. When focussed by a microscope objective, a femtosecond laser pulse induces nonlinear absorption phenomena (a combination of multiphoton and avalanche ionization processes) in otherwise transparent materials, e.g. glass; in particular a localised energy deposition is achieved only in a small volume around the focus, where the intensity is the highest. The deposited energy causes a permanent structural modification of the material. By moving the laser focus inside the substrate one can then define modified microstructures in three dimensions. Femtosecond lasers can induce three kinds of modification in fused silica according to the laser fluence [S1]: (i) refractive index changes for optical waveguide writing; (ii) formation of nanocracks for microchannel fabrication with chemical etching; (iii) microexplosions leading to laser ablation. The second type of modification is used in the current work as it allows the fabrication of microchannels of arbitrary shape and directly buried inside the substrate [S2]. The fabrication of microchannels by femtosecond laser irradiation followed by chemical etching (FLICE) is a powerful technique that has the following main advantages: a) it is a maskless technique hence allows rapid prototyping of novel configurations; b) it creates directly buried microchannels, without the need for sealing with a cover glass; c) it is a three dimensional technology, thus allowing to fabricate arbitrary designs in 3-D.

The FLICE technique applied to fused silica consists of two steps: 1) irradiation of the sample with focussed femtosecond laser pulses (Fig. 1a); 2) etching of the laser modified zone by a hydrofluoric acid (HF) solution in water (Fig. 1b). The irradiation step does not remove the material but creates nanocracks self-aligned orthogonally to the laser polarisation. These nanocracks allow diffusion of the etchant solution along the irradiated path and increase the selectivity of the etching process by a factor of 100.

Different geometries of channel network have been explored in the experiments presented in this paper; an example is the junction between several microchannel. Figure 2a shows a glass chip where several junctions have been fabricated with a different number of crossing arms, i.e. 6, 5 and 3 in the three rows respectively. A microscope image of one complete structure (Fig. 2b) clearly shows that the microchannel shape is not cylindrical but conical. This is a well known feature of microchannels fabricated by the FLICE technique [S3], which can be compensated if needed [S2]. However, in the present application this feature is advantageous since we wanted small channels in the junction (in the order of 30-50  $\mu\text{m}$  diameter) to easily localise the defects but reasonably large access holes (about 300  $\mu\text{m}$  diameter) to easily fill them and reduce the risk of clogging the channels. The 3D tapering of the channel to satisfy these two requirements was automatically achieved

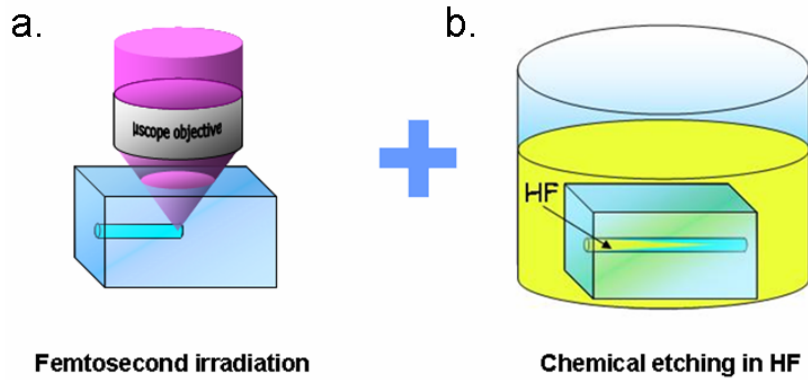


Figure 1: Schematic representation of the FLICE technique. a. Femtosecond laser irradiation of a buried pattern; b. Wet etching of the irradiated pattern in hydrofluoric acid (HF) solution.

with the FLICE technique.

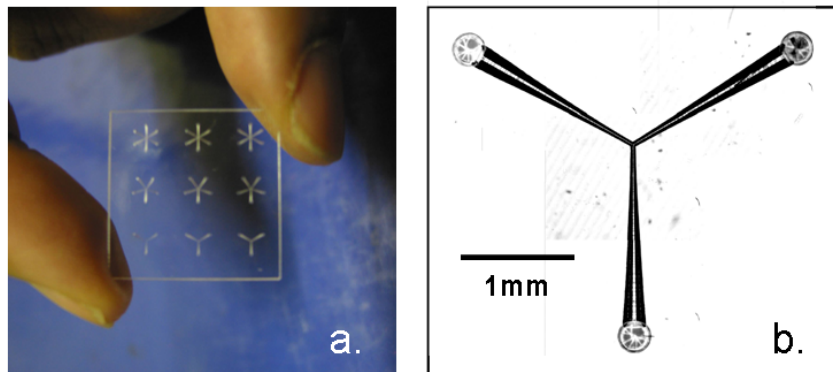


Figure 2: a. Photograph of a fused silica chip containing several microfluidic junctions with different number of arms. b. Microscope image of a three-arms microfluidic junction.

As mentioned before, the main advantage of the FLICE technique is its capability to create structures in 3D. Taking advantage of this ability we fabricated in the volume of a fused silica substrate a network of inter-crossing channels arranged as a cubic lattice. However, observation of the liquid crystal inside the microchannels would be quite difficult in this structure since the horizontal channels in the shallowest layer would mask those at a deeper level and the vertical channels would only be seen in their cross-sections. In order to improve the visualization of the structure when looking for point defects along the channels we decided to skew the cube horizontally by  $250\mu\text{m}$  along the diagonal of the cube base (see Fig. 3). In this way, the structure consists of 3 layers in depth, each separated from the other by  $200\mu\text{m}$  and the shallowest one buried  $200\mu\text{m}$  below the top surface of the sample. Each layer consists of a square grid with  $200\mu\text{m} \times 200\mu\text{m}$  openings.

Each node of the grid is then connected to the corresponding one in the layer above/below by a tilted microchannel, which can be inspected from a top view.

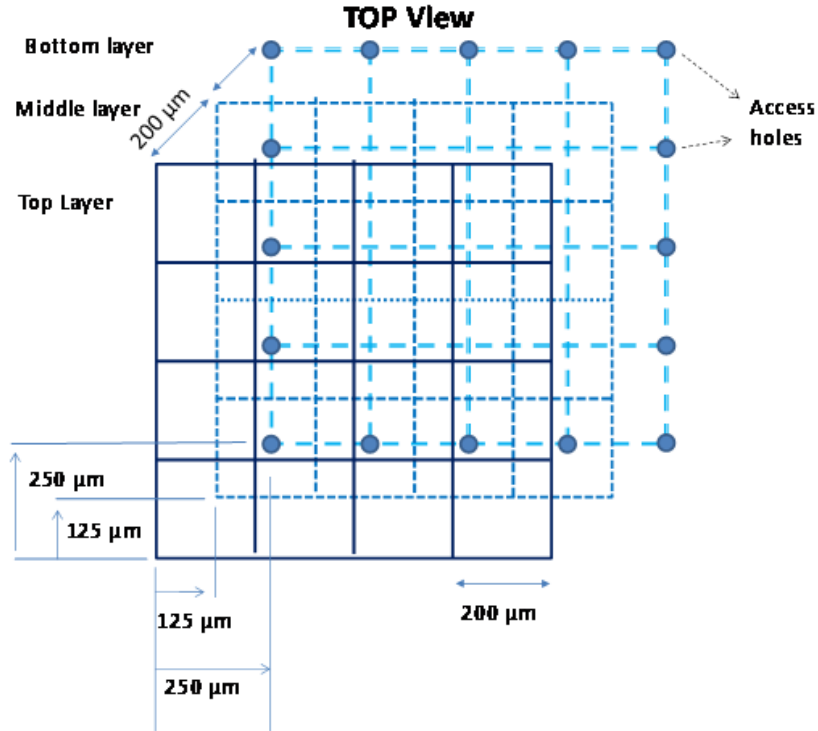


Figure 3: Schematic of the 3D structure from a top view. It can be considered as a cubic lattice skewed horizontally along the diagonal of the cube base. The nodes of each layer are connected to the corresponding ones of the layer above/below by tilted channels that are not shown in the figure for clarity.

The fabrication of the 3D structures is performed with the same technology used for the 2D structures discussed above. In particular, to facilitate the uniform HF etching of the irradiated 3D structure, the bottom layer of the structure is connected by 16 access holes to the top surface (also shown in Fig.3), where the acid can start to penetrate. The structure is etched for 45 minutes and this creates microchannels with  $\sim 40\mu\text{m}$  diameter.

## 2 Liquid crystals in capillaries

This procedure leads to homeotropic anchoring, as easily detectable along the cylindrical portions of the channels, where CCN47 adopts the escape radial (ER) configuration. As the NLC is cooled through the NI phase transition, the system undergoes, in each channel, a symmetry breaking event related to the choice of escape direction. This aspect

is very important in identifying the various configurations of the LC at the crossing point between channels. In order to explore the possible spontaneous configuration of NLC in the samples, the heating/cooling process was repeated various times over several days. Each time, after annealing at high temperature, the arrangement of topological defects and the orientation of LC in the channels was not correlated with the previous arrangement and it was not dependent on the thermal history of the sample.

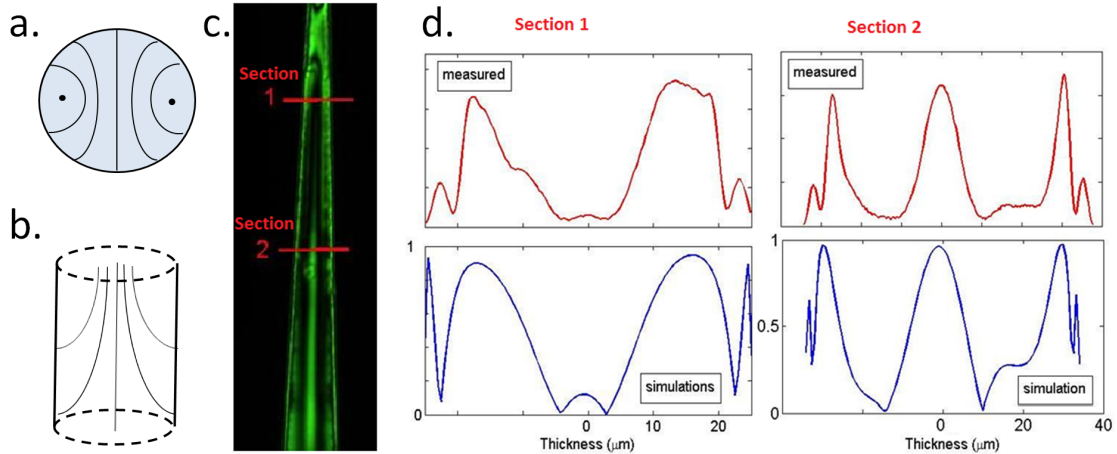


Figure 4: a. Planar polar (PP) configuration of the nematic director in a section of a capillary. The two dots correspond to disclination lines. b. Escape radial (ER) configuration inside a channel. The nematic director starts perpendicular to the channel axis, then it rotates and becomes parallel to the channel axis in the centre of the channel. c. Image of a channel with a conical section under crossed polarisers. d. Theoretical prediction (top figures) in good agreement with experimental data (bottom figures) for two sections of the channel shown in b. Both in b. and c., the channel axis is oriented at an angle of  $45^\circ$  with respect to the polariser and the analyser.

The observation of the NLC in a capillary between crossed polarisers gives rise to a complex pattern of lights and shadows, which must be interpreted according to the orientation of the nematic vector in the capillary. The director orientation of NLC with homeotropic anchoring inside capillaries was extensively studied by Crawford et al [S5], and Peroli and Virga [S4]. The two main configurations are either the planar polar (PP) or the escape radial (ER) configuration, shown respectively in figure 4 a and b. The latter configuration is expected in large channels, with diameter bigger than a few microns. In the ER channels, the nematic vector is perpendicular to the channel axis close to the channel walls (because of the homeotropic anchoring) and then escapes along the channel axis, becoming parallel to it in the centre of the channel. Knowing the functional form of the nematic director across the channel, it is possible to calculate the theoretical predictions on the propagation of polarised light across a birefringent medium for all relative positions of the polariser, analyser and channel axis. In figure 4c the

image of a channel between crossed polarisers is shown. From the image it is possible to calculate the intensity profile of the transmitted light across each section and compare it to the predictions of the theoretical models. In order to calculate the theoretical profile, a Matlab programme was developed: the programme calculates the propagation of light with Jones matrices method through a slab of birefringent material (CCN47 ordinary and extraordinary refractive indexes are used) where the orientation of the nematic director has the functional form predicted by Virga [S4]:  $n = \cos \phi e_r + \sin \phi e_z$  where  $n$  is the nematic director,  $e_r$  and  $e_z$  the radial and axial versors in cylindrical coordinates, respectively, and the angle  $\phi$  is given by  $\phi(r, \theta, z) = \pi/2 - 2 \arctan(r/R)$  where  $R$  is the cylinder radius. This method is explained in detail in Ref. [S6]. Figure 4d shows that the theoretical predictions are in agreement with the measured profile of light intensity, thus confirming the good homeotropic alignment of the NLC on the channel walls and the escape radial configuration. Although the theoretical results strictly hold for cylindrical channels, we could apply them also to the conical shapes, simply considering the right width of each section of the channel.

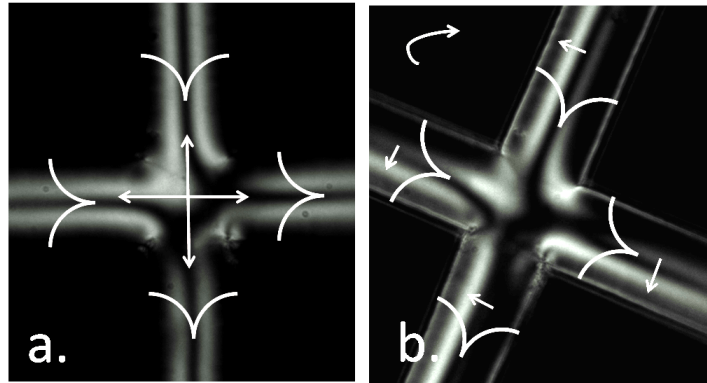


Figure 5: Node with 4 channels. In the figure the *In* and *Out* directions of the channels are highlighted. It can be seen that the dark area which appears in the centre of the channels in a. (channel axis parallel to polariser) slightly shifts in b. (channel axis at  $25^\circ$  with respect to the polariser direction). For the *In* and *Out* channel the direction of the shift is different with respect to the reference direction going from the node to the end of the channel (as indicated in a.)

In the cylindrical channels, it is also very important to identify the direction of the escape, either towards the node (*In*) or outwards (*Out*). A simple technique is observing the birefringence pattern of the cylinder with the channel axis forming an angle around  $22^\circ$  with respect to the polariser direction. If the channel axis is parallel to the transmission axis of the polariser (or the analyser), the centre of the channel appears dark because the LC are oriented along the channel axis. The brightness is maximum between the channel centre and the channel walls, where the LC are twisted by a  $45^\circ$  angle. As the channel axis rotates, the dark region shifts, and the shift direction depends on the orientation of the escape inside the channel, as shown in figure 5. A simple rule is: considering as a

reference the direction which goes from the node to the end of the channel, a clockwise rotation induces a right-shift of the dark area if the channel escape is *Out* and a left-shift if the escape is *In* (towards the node). If the rotation is counterclockwise the directions are reversed.

Another method, particularly useful in the observation of the 3D network, is to insert an extra  $\lambda/4$  filter in addition to the crossed polarisers (without the green filter). This produces a shift in the wavelength of the transmitted light which depends on the direction of the ER: with one ER direction the color shifts to higher wavelengths (red-shift), while with the opposite ER it shifts towards shorter wavelength (blue-shift).

### 3 Displacing defects

With the application of an electric field or of a mechanical pressure it is possible to change the position of the point defects in the glass microchannels. Figure 6 shows such an example on a 3D structure. The glass slab containing the microstructure was sandwiched between two ITO coated glasses and an electric field of 200 V was applied between these two glasses, then removed. The gap between them was given by the thickness of the glass slab, i.e. almost 1mm, therefore the electric field in between the plates is not very high. Nevertheless, in several cases the electric field was able to move defects around the channels.

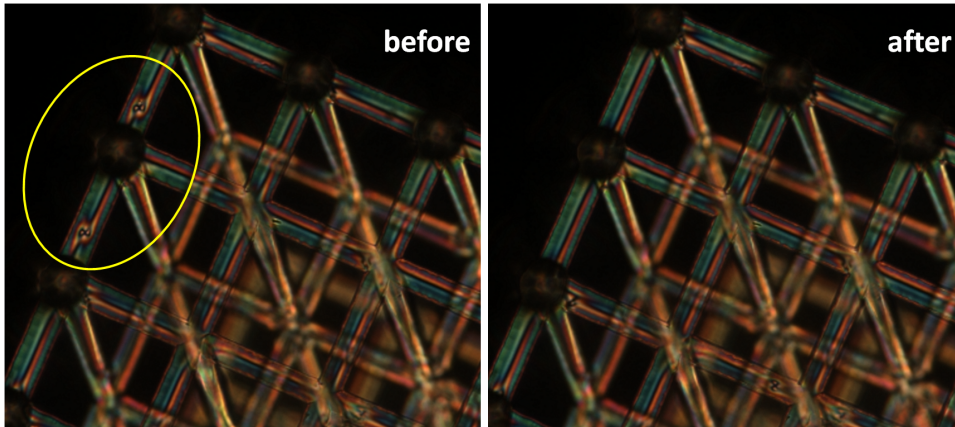


Figure 6: Switching defects with an electric field. The two panels show the same sample viewed between crossed polarisers before and after an electric field applied for a few seconds and removed. The yellow line encircles the area from which two point defects were clearly moved.)

## References

- [S1] Rafael R. Gattass and Eric Mazur. Femtosecond laser micromachining in transparent materials. *Nature Photon.*, 2(4):219–225, 2008.
- [S2] K. C. Vishnubhatla, N. Bellini, R. Ramponi, G. Cerullo, and R. Osellame. Shape control of microchannels fabricated in fused silica by femtosecond laser irradiation and chemical etching. *Opt. Express*, 17(10):8685–8695, 2009.
- [S3] V. Maselli, R. Osellame, G. Cerullo, R. Ramponi, P. Laporta, L. Magagnin, and P. L. Cavallotti. Fabrication of long microchannels with circular cross section using astigmatically shaped femtosecond laser pulses and chemical etching. *Appl. Phys. Lett.*, 88(19):191107, 2006.
- [S4] G. Guidone Peroli and E. Virga. Annihilation of point defects in nematic liquid crystals. *Phys. Rev. E*, 54:5235, 1996.
- [S5] G. P. Crawford, D. W. Allender, and J. W. Doane. Surface elastic and molecular anchoring properties of nematic liquid crystals confined to cylindrical cavities. *Phys. Rev. A*, 45:8693, 1992.
- [S6] M. Buscaglia, G. Lombardo, L. Cavalli, R. Barberi and T. Bellini Elastic anisotropy at a glance: the optical signature of disclination lines *Soft Matter*, 6:5434, 2010.